

Viral Structural Transition Mechanisms Revealed by Multiscale Molecular Dynamics/Order Parameter eXtrapolation Simulation

Yinglong Miao, Peter J. Ortoleva

Center for Cell and Virus Theory, Department of Chemistry, Indiana University, Bloomington, IN 47405

Received 30 June 2009; revised 6 August 2009; accepted 6 August 2009

Published online 2 September 2009 in Wiley InterScience (www.interscience.wiley.com). DOI 10.1002/bip.21299

ABSTRACT:

On the basis of an all-atom multiscale analysis theory of nanosystem dynamics, a multiscale molecular dynamics/order parameter extrapolation (MD/OPX) approach has recently been developed. It accelerates MD for long-time simulation of large bionanosystems and addresses rapid atomistic fluctuations and slowly varying coherent dynamics simultaneously. In this study, MD/OPX is optimized and implemented to simulate viral capsid structural transitions. Specifically, 200 ns MD/OPX simulation of the swollen state of cowpea chlorotic mottle virus capsid reveals that it undergoes significant energy-driven shrinkage in vacuum, which is a symmetry-breaking process involving local initiation and front propagation. © 2009 Wiley Periodicals, Inc. *Biopolymers* 93: 61–73, 2010.

Keywords: structural transition mechanisms; all-atom multiscale; molecular dynamics/order parameter extrapolation (MD/OPX); cowpea chlorotic mottle virus (CCMV); symmetry-breaking; local initiation; front propagation

Correspondence to: P. J. Ortoleva; e-mail: ortoleva@indiana.edu
Contract grant sponsors: National Institutes of Health (Stanford University via SimBios), National Science Foundation (Collaborative Research in Chemistry Program), NIH National Institute of Biomedical Imaging and Bioengineering, Indiana University College of Arts and Sciences, and METACyt project (Center for Cell and Virus Theory)

© 2009 Wiley Periodicals, Inc.

This article was originally published online as an accepted preprint. The “Published Online” date corresponds to the preprint version. You can request a copy of the preprint by emailing the Biopolymers editorial office at biopolymers@wiley.com

INTRODUCTION

Many viruses undergo structural transitions (STs) in response to changes in the microenvironment, such as temperature, pH, ionic strength, and cation concentrations. For example, native cowpea chlorotic mottle virus (CCMV) or its empty capsid swells dramatically as pH is increased from 5.0 to 7.5 in the absence of divalent cations at low ionic strength ($I = 0.2$ M),^{1–4} and disassembles at high ionic strength ($I = 1.0$ M).¹ Nudaurelia capensis ω virus (N ω V)^{5,6} and HK97 bacteriophage⁷ undergo STs during capsid maturation. Poliovirus undergoes irreversible STs on maturation or receptor-mediated cell entry.^{8,9} STs and disassembly play key roles in viral life-cycle events, including virus attachment to cell membranes and genome release from the viral capsid into a host cell. As characterized quantitatively via electron cryomicroscopy (cryoEM) and X-ray crystallography, STs in viral capsids are typically accomplished through a series of distinct steps involving intact translation and rotation of protein structural units (e.g., pentameric and hexameric capsomeres), whereas others, as in poliovirus and N ω V, are triggered by irreversible bond cleavage of capsid proteins.

Theoretical approaches have been applied to simulate viral properties and dynamics, including (1) computational molecular dynamics (MD)^{10–12}; (2) uncoupled coarse-grained models^{13,14}; (3) symmetry-constrained models¹¹; (4) normal mode analysis (NMA)^{15–17}; and (5) Poisson-Boltzmann (PB) approaches^{18–21} as reviewed earlier.^{21–23} Although these approaches reveal interesting features of viral stability and dynamics, they do not meet the challenge of whole-virus simulation for one or more of the following reasons. They (1) are limited to biologically irrelevant timescales; (2)

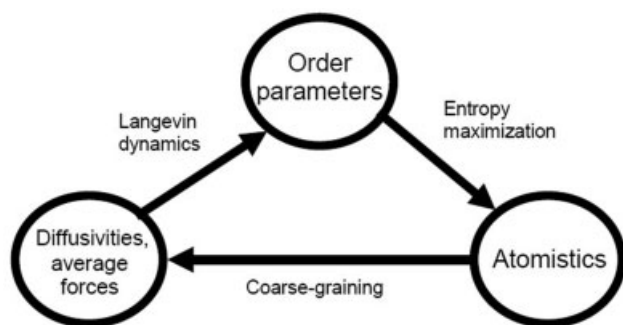


FIGURE 1 Order parameters characterizing nanoscale features affect the probability of atomistic configurations, which, in turn, mediate the forces driving order parameter dynamics.

require recalibration with each new application; (3) lack the atomistic detail needed to address viral interaction with cell receptors or drug molecules; (4) impose symmetry constraints incompatible with the local, asymmetric nature of drug or cell receptor interaction at selected sites on the virus; (5) use small amplitude vibration theory and thereby miss the nonlinear nature of STs; (6) ignore the highly dissipative nature of nanoscale dynamics (i.e., the important role of frictional forces); and (7) miss the interscale feedback whereby nanoscale structural variables affect the statistical distribution of atomic scale fluctuations, which, in turn, mediate the entropic and free energy effects that drive the dynamics of the nanoscale features^{22,24} (Figure 1). This feedback loop is central to a complete understanding of nanosystems and the true nature of their dynamics.

The essence physical picture of viruses is that they are nanosystems composed of millions of atoms, which involve processes taking place across widely separated time and length scales. It is natural to adopt a multiscale approach to study their dynamics. Multiscale analysis has been of interest since work on Brownian motion by Einstein. It was shown that the wandering of a nanoparticle arises because of the interplay of short-scale random collisions and the large-scale, slow motions of the whole nanoparticle created by the separation in the magnitude of the mass of an atom versus that of the nanoparticle. In earlier studies, Fokker-Plank and Smoluchowski equations are derived from the Liouville equation for nanoparticles without internal atomistic structure.^{25–32} The development of projection operators³³ is not directly applicable because it (1) requires integration over atomistic configurations and thereby makes it difficult to capture internal structure and (2) involves memory kernels that are not readily evaluated using standard MD. We have advanced the multiscale approach to develop an all-atom multiscale analysis (AMA) theory for dynamical nanosystems²² by (1) accounting for atomic scale fluctuations of the system inter-

nal structure; (2) introducing general, automatically generated collective modes and order parameters (OPs); (3) constructing ensembles of atomic configurations constrained to fixed values of the slowly varying OPs, as needed to construct thermal-average forces and friction/diffusion coefficients for their stochastic equations; (4) applying perturbation expansion to the solution of N -atom Liouville equation in terms of a smallness parameter (length or time scale ratio of one atom to the entire system); and (5) deriving stochastic equations (Fokker-Plank or Smoluchowski) for the probability density of coarse-grained system OPs. The AMA approach captures the cross-talk between the OPs and atomistic variables rigorously as suggested in Figure 1,^{22,24,34,35} and provides the conceptual framework for our whole-virus simulation approach.

A multiscale coupling approach bridged the nano and mesoscopic scales by embedding a nanoscale level system into a mesoscopic continuum.^{36,37} In the case of membrane simulations, MD was used to calculate material properties to parameterize an elastic membrane model; the surface tension of a local region is then calculated and applied back to the corresponding membrane zone as a boundary condition for its MD simulation. This multiscale coupling approach describes the interface between a local region of a mesoscopic system and the remainder of the system. However, it does not capture the cross-talk between the rapid atomistic fluctuations and coherent nanoscale modes during system structural changes, the nonlinearity of the membrane, and the highly dissipative nature of the system in a self-consistent manner. In contrast, these facets are addressed in our AMA approach, which accounts for the feedback loop of Figure 1.

On the basis of the concepts from AMA theory of nanosystem dynamics, we developed a multiscale MD/order parameter eXtrapolation (MD/OPX) approach for simulating viruses and other large bionanosystems.²³ In the implementation, OPs constructed with orthogonal polynomials of atomic coordinates of a reference configuration are introduced to capture the system slowly varying nanoscale features. Replica short MD runs with random atomic velocity initializations are implemented to estimate the ensemble-average rate of change in OPs, which is then used to extrapolate the system over a time period that is much longer than the 10^{-14} s timescale of fast atomic vibrations and collisions. Because the timescale for the evolution of OPs is much larger than that of atomic vibrations and collisions, the OPX time can be many orders of magnitude greater than the MD simulation timestep. The resulting MD/OPX algorithm greatly accelerates MD, and its underlying all-atom description of nanosystems enables the use of a universal interatomic force field, avoiding recalibration with each new application as needed for coarse-grained models. MD/OPX addresses rapid

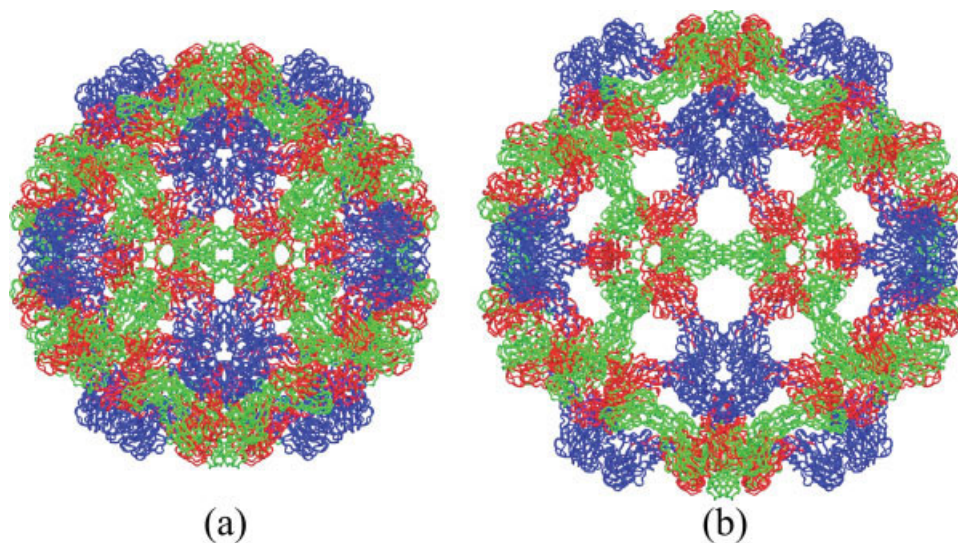


FIGURE 2 (a) Native CCMV capsid organized in 12 pentamers and 20 hexamers with 5 A (blue) subunits in each pentamer and 3 B (red) and 3 C (green) subunits in each hexamer, and (b) its swollen state generated through rigid-body translation and rotation of the pentamers and hexamers according to the expansion scheme proposed by Liu et al.⁵⁰

atomistic fluctuations and slowly varying coherent dynamics of nanosystems simultaneously.

The equation-free multiscale analysis (EFM) approach developed by Kevrekidis et al.³⁸ shares much of the flavor of MD/OPX, i.e., short bursts of MD simulations can be used to extrapolate coarse variables (i.e., OPs here) over large time intervals and thus project the system over long time. It has been applied to an alanine dipeptide for MD study by using the dipeptide dihedral angle ($N-C_{\alpha}-C-N$) as its coarse variable.³⁹ However, the dipeptide is a very small system, and its dihedral angle does not seem to be a slow variable and therefore cannot be extrapolated over long time. PCA has been used to reduce the dimensionality of MD trajectories for analyzing large-scale structural changes, but PCA modes calculated for consecutive time windows of MD trajectories have been shown to display small similarities.^{40–43} This proves that they fail to capture system coherent motions over long time. It is thus not reliable to use PCA modes obtained from short MD runs to facilitate the long-time simulation of nanostructures because of limited sampling of long-range correlations and forced orthogonalization of PCA modes.^{44–46} In contrast, collective modes and order parameters automatically constructed with basis functions of atomic positions of a reference configuration or atomic displacements between two known configurations capture slow, nanoscale dynamics of viruses and other bionanosystems and serve as a starting point for an AMA that justifies MD/OPX.⁴⁰

In this study, MD/OPX is applied to simulate viral STs by taking CCMV capsid as our model system. CCMV is a mem-

ber of the bromovirus group of the Bromoviridae family. Its genome consists of four positive-sense single-stranded RNA molecules, two of which are encapsulated separately in two virions, and the remaining two are packaged together into a third type of particle. Because the purified RNA and coat proteins of CCMV can reassemble *in vitro* to produce infectious virions⁴⁷ and the empty CCMV capsid assembled from its protein subunits displays many behaviors similar to those of the complete virus,^{3,48} it is an excellent system for studying protein–protein and protein–RNA interactions and for investigating the mechanisms of viral STs, self-assembly, and disassembly.

RESULTS AND DISCUSSION

Although modules have been developed in MD/OPX to account for water molecules and ions to simulate nanostructures solvated in aqueous media,⁴⁹ we are focused on simulating CCMV capsid in vacuum (i.e., gas phase) and studying its ST mechanisms with long-time dynamics captured in this study. We first investigate the stability of the native and swollen states of CCMV capsid through short-time MD simulations. With analysis results showing that the capsid-native state becomes stable after short, small shrinkage, while its swollen state keeps shrinking even at the end of 10 ns MD simulation, MD/OPX is implemented to simulate the long-time dynamics of swollen CCMV capsid. The ST mechanisms of swollen CCMV capsid during its shrinkage are discussed.

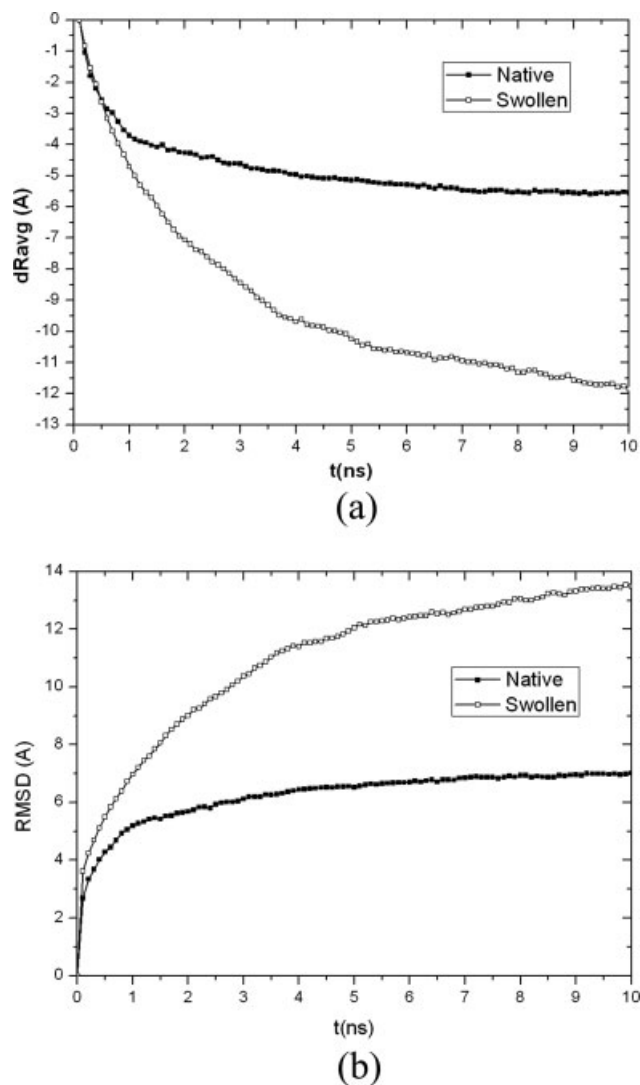


FIGURE 3 Ten-nanosecond MD simulation of the native and swollen states of CCMV capsid: (a) time courses of the decrement in capsid average radius from their initial structures and (b) RMSD of atomic positions between their trajectory snapshots and the initial structures.

Insights into CCMV Capsid Stability Through Short-Time MD Simulations

Figure 2 shows ribbon representations of the native and swollen states of CCMV capsid. Native CCMV capsid (Figure 2a) is composed of 180 chemically identical protein subunits that form a 286-Å diameter icosahedral shell displaying a $T = 3$ quasi-symmetry. Each protein subunit is composed of 190 amino acids taking three quasi-equivalent positions on the capsid surface. As such, one asymmetric unit (i.e., protomer) of the capsid includes three subunits that are colored in blue for A, red for B, and green for C in Figure 2. The icosahedral capsid can also be divided into

12 pentamers and 20 hexamers with 5 A subunits in each pentamer and 3 B and 3 C subunits in each hexamer. Native CCMV is well known to undergo a pH-induced swelling transition in host medium. In the expansion scheme proposed by Liu et al.,⁵⁰ its swollen state (Figure 2b) can be generated by taking the pentamers and hexamers through rigid-body transformations (see Materials and Methods section).

To identify key elements for performing long-time MD/OPX simulation of CCMV capsid, NAMD was first implemented to run short-time MD simulations (10 ns) on its native and swollen states for insights into their structural stability (see Materials and Methods section). With 10 ns MD trajectories of the two structures obtained, frames taken for every 0.1 ns were superimposed to their simulation starting configurations, respectively, to remove overall translation and/or rotation of the capsid. Then, change in the capsid size was analyzed by calculating the decrement of capsid average radius, i.e., the average distance of non-hydrogen atoms in capsid backbone to their center of mass (COM), from their initial values. The calculation results plotted in Figure 3a show that the native state of CCMV capsid shrinks during the first 3 ns of simulation with its average radius decreased by 4.6 Å and becomes stable afterward, whereas its swollen state shrinks much more significantly with the capsid average radius decreased by 11.8 Å along the trajectory and still keeps shrinking at the end of the simulation at 10 ns. Structural changes in two states of the capsid can also be verified by observing time courses of the root mean square deviation (RMSD) of atomic positions between their trajectory snapshots and the initial configurations as shown in Figure 3b. RMSD for the capsid-native state is found to increase from 0 to 6 Å during 3 ns and level off afterward, whereas RMSD for its swollen state increases more dramatically (8.4 Å at 3 ns) and still displays increasing trend at 10 ns. Therefore, native CCMV capsid tends to be stable after short, small shrinkage in vacuum, whereas its swollen state undergoes shrinkage over a time period that is expected to be much longer than 10 ns. With this, MD/OPX is implemented to simulate the long-time dynamics of swollen CCMV capsid in the following.

Shrinkage of Swollen CCMV Capsid in Vacuum Captured by Long-Time MD/OPX Simulation

As explained in Materials and Methods section, atomic coordinates of a reference configuration or atomic displacements of two reference configurations were used to construct system OPs by using their orthogonal polynomials or harmonic

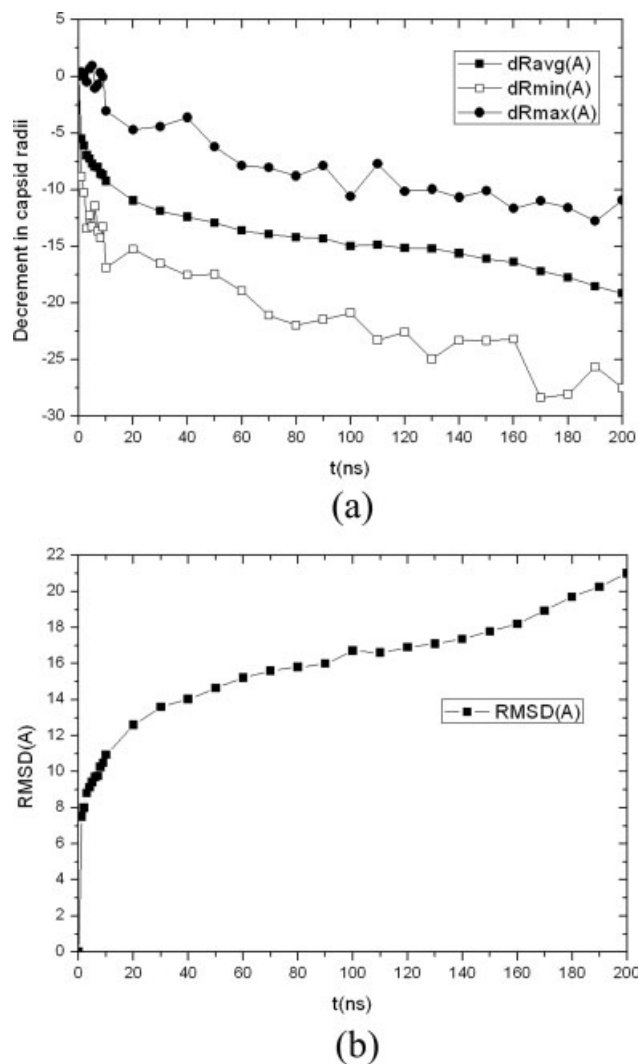


FIGURE 4 Two hundred-nanosecond MD/OPX simulation of the swollen CCMV capsid: (a) time courses of the decrement in the average, minimum, and maximum radii of the capsid backbone from the simulation starting structure, and (b) RMSD of atomic positions between capsid snapshots along the trajectory and the initial structure.

functions,⁴⁰ with which MD/OPX demonstrated through our previous study²³ was optimized and implemented to simulate swollen CCMV capsid in vacuum with 200 ns dynamics captured.

Analysis on the simulation output trajectory shows that swollen CCMV capsid shrinks with the average radius of its backbone decreased by 19.15 Å during 200 ns (Figure 4a). It thickens by 11 Å during shrinkage and undergoes fluctuations as indicated by the time courses of the decrement in the minimum and maximum radii of the capsid backbone (i.e., the minimum and maximum distances of capsid backbone atoms to the capsid COM). RMSD of atomic positions

between capsid snapshots along the trajectory and its starting structure increases from 0 Å to 21.01 Å in 200 ns (Figure 4b). The capsid is found to shrink fast in early stage of the simulation with quick drop in the capsid average radius and sharp increase in the capsid RMSD, and the shrinkage slows down as the capsid approaches its near-equilibrium state that is expected to be close to the native.

To identify characteristics of the shrinkage of swollen CCMV capsid in vacuum, interior view of its back half (selected through $z < 0$ with the capsid centered at origin) for the simulation starting and final structures are shown in Figures 5a and 5b. In Figure 5c, arrows are drawn from subunit COMs of the capsid initial structure to their final positions. It can be observed that pentamers and hexamers in the capsid translate radially inward and rotate in a clockwise manner during capsid shrinkage. As a result, the openings between the capsomeres along the quasi-threefold axes become small, heading toward the “closed” native state. This acts as a reverse process to the pH-induced expansion of native CCMV capsid into its swollen state in host medium.

To examine the suitability of considering pentamers and hexamers as rigid units during CCMV capsid shrinkage, we choose a pentamer and a hexamer from the capsid, calculate their RMSD of atomic positions between trajectory snapshots and their initial configurations after structure superimposition, and compare them with that for the entire capsid. Results in Figure 6a show that RMSD for a pentamer or a hexamer increases to ~ 5 Å in 1 ns and displays slight changes afterward, whereas RMSD for the entire capsid keeps increasing through the simulation as described above. This indicates that the pentamer and hexamer adjust their internal structures quickly during early stage of the simulation and become stable afterward during shrinkage of the capsid, which then can be considered as a process of rearranging the capsid pentamers and hexamers by overall translation and rotation. Calculations on the average translation distances and rotation angles of 12 pentamers and 20 hexamers during capsid shrinkage give us quantitative results as follows. As shown in Figures 6b and 6c, pentamers translate radially inward by 20.11 Å on average during 200 ns, and hexamers translate by 18.84 Å, and they undergo clockwise rotation by about 6.19° and 3.26°, respectively, with moderate fluctuations. The simulated capsid shrinkage transforms pentamers and hexamers in directions that are reverse to those applied to generate the swollen capsid from its native state.

Although above results are obtained by averaging translation distances and rotation angles over the pentamers and hexamers, a further step is to look into the transformation of capsomeres individually during capsid shrinkage. To do this,

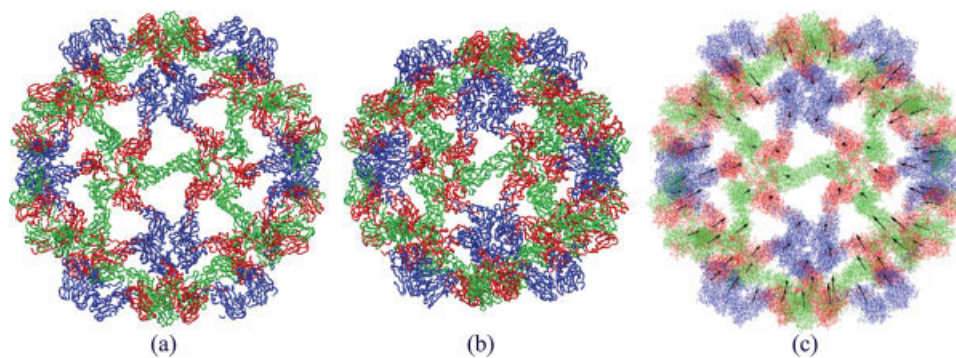


FIGURE 5 Interior views of (a) swollen CCMV capsid, (b) the final structure of 200 ns MD/OPX simulation, and (c) the COM displacements of protein subunits from their initial configurations to the final that depict shrinkage of the capsid.

12 pentamers from P1 to P12 and 20 hexamers from H1 to H20 are first labeled in icosahedral CCMV capsid according to the scheme provided in Figure 7a. Then, their COM translation distances from the initial positions are plotted as a function of time in Figures 7b and 7c for pentamers and hexamers, respectively. Results show that the 12 pentamers do not translate at the same speed with P11 and P7 moving the fastest, P8 and P12 the slowest, and the others between through most of the simulation time. Notice that P1 and P3 lead the translation of pentamers from 170 ns to the end of simulation. For hexamers, H13, H20, and H4 are in the fast-moving group, whereas H15 and H17 belong to the slowly moving. By examining the distribution of these capsomeres in Figure 7a, one can find that the fast-moving hexamers and pentamers tend to be neighboring capsomeres, e.g., H13 to P11 and H20 to P7, and similarly for the slowly moving ones, e.g., H15 to P8 and H17 to P12. This implies that the motions of capsomeres are largely correlated and that it results from the structural features of CCMV capsid. According to CCMV structural studies,² the carboxyl terminal arms of protein subunits in its pentamers and hexamers are known to “invade” their neighboring capsomeres, through which the capsomeres are tightly intertwined with each other. Thus, capsomeres would undergo cooperative motions with strongly coupled allosteric interactions. As a result, swollen CCMV capsid does not preserve its icosahedral symmetry during shrinkage and it involves symmetry-breaking cooperative motions of the capsomeres.

Mechanisms of Viral Capsid ST

As indicated above, shrinkage of swollen CCMV capsid in vacuum involves large-scale rearrangements of the pentamers and hexamers and icosahedral symmetry is not preserved during the transition. Symmetry-breaking is a well-known feature in the self-organization and structural phase transi-

tions of macroscopic systems.^{51,52} For example, martensitic transformations that are characterized by a collective movement of large numbers of atoms occur in solid-state materials, such as iron and metal alloys, and they are found to change system symmetries.^{53,54}

It has been suggested that STs in viral capsids are analogous to structural phase transitions in macroscopic solids and thus methods in solid-state physics can be applied to viral capsids. On the basis of this hypothesis, viral capsid STs were studied with phenomenological continuum theory adapted from the Ginzburg-Landau model of soft-mode solid structural phase transitions. The theory predicts that the STs are characterized by a pronounced softening of the capsid elasticity and external force applied by an AFM probe can drive a capsid into a state of phase coexistence where the capsid is partly in the immature state and partly in the mature state with two of them separated by a phase boundary.⁵⁵

To understand the mechanisms of viral capsid ST, allosteric coupling has been proposed by Caspar.⁵⁶ It states that the conformational change in one capsid subunit triggers that in neighboring subunits, which then induces structural changes in more subunits across the capsid. Such cooperative conformational changes display symmetry-breaking behaviors as found for pentamers and hexamers in swollen CCMV capsid during its shrinkage. This is common to STs of many other viral capsids during maturation as well.^{57,58}

Experimental and theoretical studies on HK97 bacteriophage capsid show that it undergoes expansion from a metastable procapsid (prohead) to a mature icosahedral capsid (head) through three steps⁵⁹: (1) local refolding of capsid subunit N-terminal arms; (2) global expansion of the capsid involving large-scale rearrangements of capsid subunits; and (3) additional subtle and slow structural changes contributing to cross-linking of capsid subunits that stabilize the

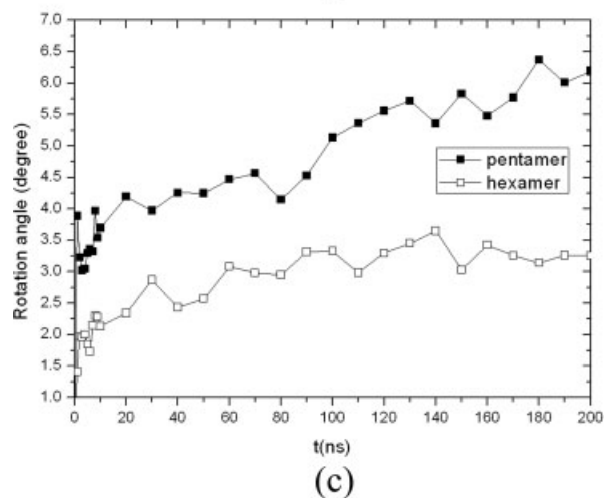
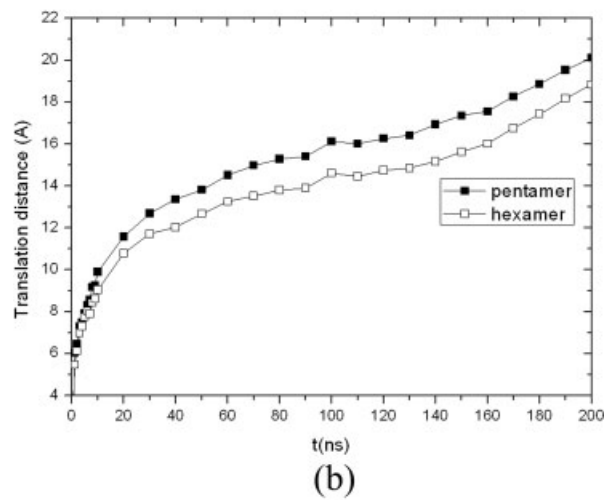
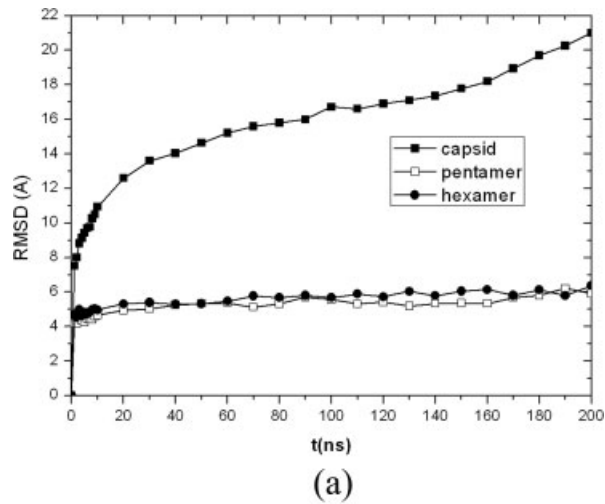


FIGURE 6 (a) RMSD of atomic positions for a selected pentamer and a hexamer (see Figure 7a for P1 and H1) between trajectory snapshots and their initial configurations in comparison with that for the entire capsid, (b) the average COM translation distance as a function of time for pentamers and hexamers, and (c) time courses of the average rotation angle for pentamers and hexamers calculated through fitting their structures to the initial configurations.

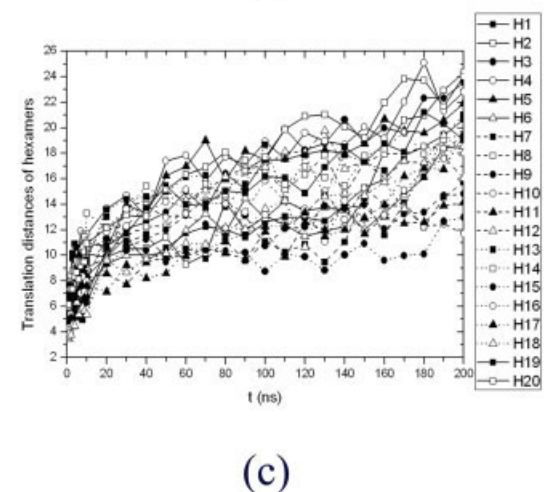
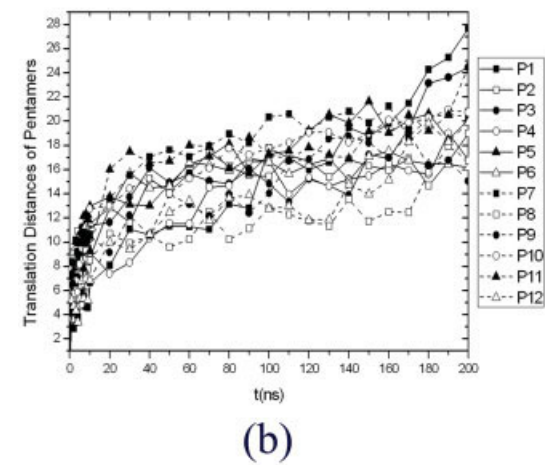
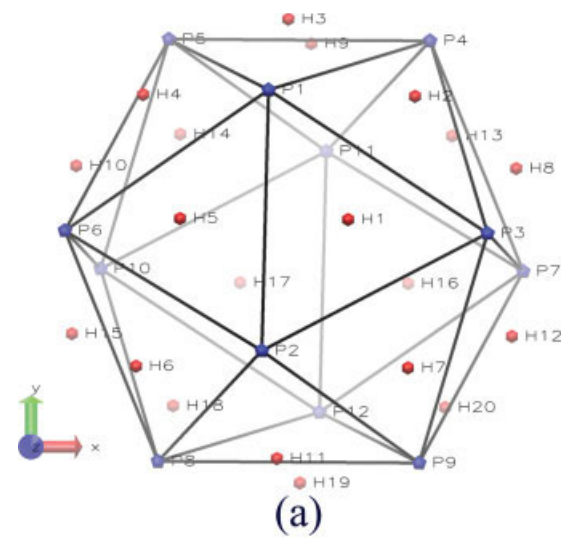


FIGURE 7 (a) Schematic representation of icosahedral CCMV capsid with 12 pentamers (blue pentagons) labeled from P1 to P12 and 20 hexamers (red hexagons) from H1 to H20, and time courses of the COM translation distance of (b) pentamers and (c) hexamers from their original positions.

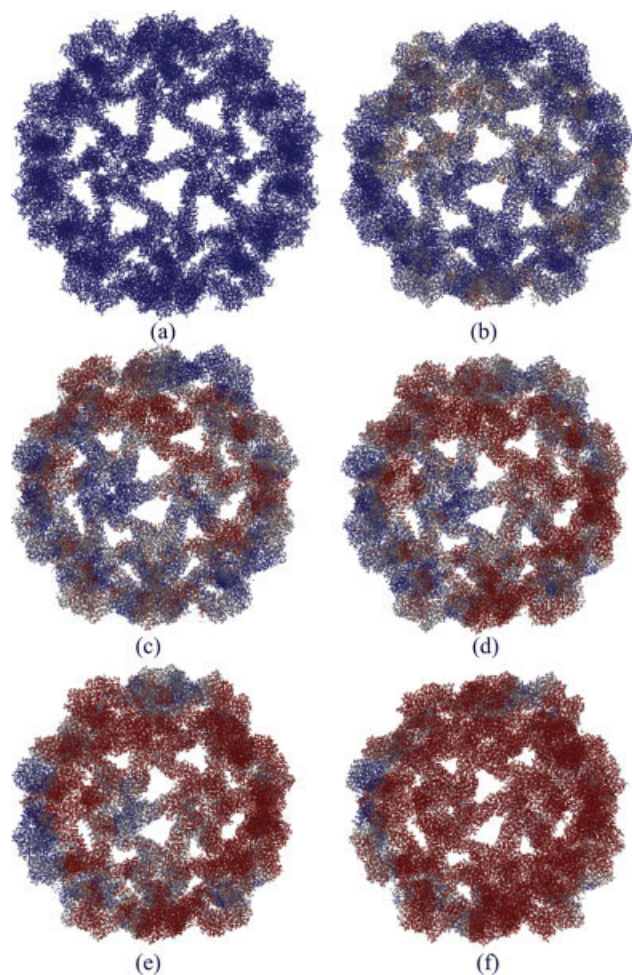


FIGURE 8 Interior view of the capsid shrinkage trajectory snapshots with atoms colored by their displacements from the original positions in a BWR color scale (0 Å for blue, 24 Å for red, and white as the midpoint): (a) initial state with all atoms in blue, (b) 5 ns, (c) 20 ns, (d) 50 ns, (e) 100 ns, and (f) 200 ns of simulation. It can be seen that atoms in the upper pentamer of shown trajectory snapshots (i.e., P11 as labeled in Figure 7a) start to change their color from blue to white and to red first, and then this color change propagates across the capsid. Thus, capsid shrinkage is a symmetry-breaking/front propagation process.

mature capsid. Although greatest structural changes take place during capsid global expansion, they are triggered by local refolding of the capsid subunit N-arms. This suggests that the capsid does not preserve its symmetry during the initial highly localized conformational changes and even the cooperative motions of capsid subunits during its expansion.⁵⁸ MD simulations on satellite tobacco mosaic virus (STMV)¹⁰ show that its capsid also undergoes symmetry-breaking ST. Although the complete virion (capsid embedded with RNA) deviates its shape from icosahedral symmetry with only minor, local ones over 13 ns of simulation, empty viral capsid was found to collapse, and its shape becomes

very different from the initial state after 10 ns with the icosahedral symmetry lost completely.

Although pH-induced CCMV swelling has been determined to be a first-order transition as suggested by hysteresis of CCMV in its titration curves under certain conditions⁶⁰ and pH-driven softening of capsid elasticity in AFM experiments,⁶¹ exact mechanisms of the capsid ST remain unclear.⁴ With our all-atom multiscale MD/OPX simulation of swollen CCMV capsid, we are able to obtain a microscopic view of its STs, and therefore explore the exact symmetry-breaking mechanisms during capsid shrinkage. Figure 8 shows interior view of the capsid trajectory snapshots at (a) initial swollen state; (b) 5 ns; (c) 20 ns; (d) 50 ns; (e) 100 ns; and (f) 200 ns. Atoms in the capsid are colored by their displacements from the original positions in a blue-white-red color scale (i.e., 0 Å for blue, 24 Å for red, and white as the midpoint) to investigate conformational changes in the swollen CCMV capsid. It is seen that atomic displacements are not constrained to icosahedral symmetry, i.e., atoms in the capsid do not change their colors simultaneously in a symmetry-preserving manner. Shrinkage of swollen CCMV capsid involves an “initiation and front propagation” mechanism. It starts from the upper pentamer as shown in trajectory snapshots and several other local regions of the capsid in which atoms change their colors from blue to white and to red first. This nucleation needs 20 ns to occur. The ST then propagates across the capsid seen as spreading of the red areas. The propagation of cooperative motions from one capsomere to its neighboring ones takes place on a timescale of 10 ns. Thus, the propagation speed is ~ 0.6 nm/ns with the average capsomere distance considered as 6 nm. Therefore, STs of viral capsids start

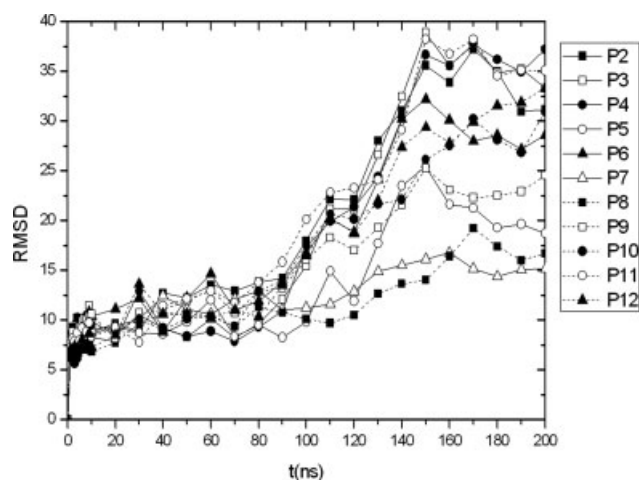


FIGURE 9 Time courses of RMSD of atomic positions between Pentamer P1 as labeled in Figure 7a and the 11 others after rigid-body transformation of P1 to the positions of other pentamers according to icosahedral symmetry.

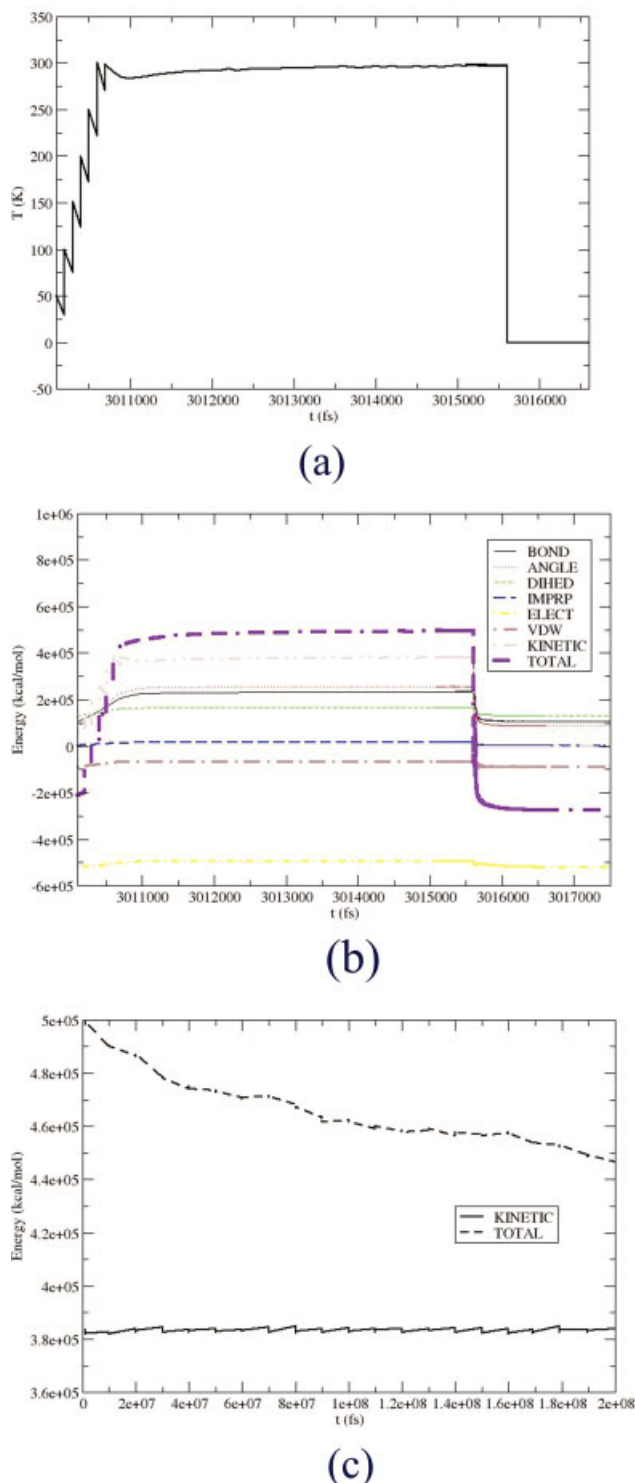


FIGURE 10 Variations of the system temperature (a) and energies (b) in one typical MD/OPX cycle capturing 3,010,100–3,075,100 fs of the simulation, and (c) the system kinetic and total energies plotted versus time during 200-ns capsid shrinkage.

with local conformational changes that break icosahedral symmetry of the capsid, followed by global structural changes that involve large-scale cooperative translations and rotations of capsid structural units (e.g., capsomeres or protein subunits) through strong allosteric interactions.

To evaluate symmetry-breaking of CCMV capsid during its shrinkage quantitatively, we calculate the RMSD of atomic positions between Pentamer 1 as labeled in Figure 7a and the 11 others after rigid-body transformation of the chosen pentamer to the positions of others according to icosahedral symmetry. These RMSDs (Figure 9) are found to increase up to about 200 ns with structural changes breaking capsid symmetry and then decrease afterward as the capsid transforms toward its near-equilibrium state (one close to the icosahedral native state). As a result, even though the initial and final states of swollen CCMV capsid have icosahedral symmetry, symmetry is not preserved during its shrinkage.

The fact that shrinkage of swollen CCMV capsid in vacuum is symmetry-breaking at first seems to conflict with prevailing thinking. For example, symmetry has been used to facilitate the simulation of icosahedral viruses by assuming symmetry is preserved during their STs.^{11,15,17} However, as with structural phase transitions in macroscopic solids, viral capsid STs start locally and then propagate across the capsid, i.e., they proceed through intermediate states that are not constrained to the capsid symmetry.⁵³ Examples of such viral symmetry-breaking STs include those induced by local interactions of viral capsids with cell receptors or antiviral drug molecules.^{9,12,62,63} Given the fact that viral capsid STs are symmetry-breaking processes, the use of symmetry-constrained models in studying the pathways and mechanisms of STs in CCMV and other icosahedral viruses is not appropriate. Particularly, the energy barrier for making coherent translations and rotations of all capsomeres or capsid subunits in the course of viral capsid STs is much greater than that for a single or local cluster of these substructures. Thus, one expects that prediction of transition time based on a symmetry-constrained model should be unphysically long.

Shrinkage of Swollen CCMV Capsid Is Energy Driven

In the following, we examine system energies for shrinkage of swollen CCMV capsid in vacuum simulated via MD/OPX. Because MD/OPX cycles are composed of short replica MD runs, projection of system configuration through extrapolation of its OPs and maturation of the OPX resulting structure by applying energy minimization, graduate heating, and short-time MD equilibration (see Materials and Methods section), and temperature control is applied all through the

simulation, we first look into variations of the system temperature and energies in one typical MD/OPX cycle.

For our analysis, the 32nd MD/OPX cycle of the simulation running from 3,010,100 fs to 3,075,100 fs with the ratio of OP timestep to the time interval of short MD runs obtained as 120 (also the average value for the entire simulation) was chosen. In Figure 10a, the system temperature was plotted as a function of time: it starts from 0 K as a result of energy minimization of the OPX resulting configuration from previous cycle, increases to 298.15 K in a six-stepwise manner as the system is heated gradually by 50 K for each of the first five steps and 48.15 K for the last step (100 fs equilibration for each temperature increase), becomes stable as the system is equilibrated to 298.15 K for 4400 fs; stays around 298.15 K under which ten 500-fs short replica MD bursts are run for calculating the ensemble-averaged rate of change in system OPs, and drops to 0 K as the atomic configuration is reconstructed with newly extrapolated OPs over 60,000 fs and energy minimization is performed. Note that for each heating step, atomic velocities are reinitialized for the system to reach a higher temperature, after which there is a slight drop in system temperature because of conversion of the system kinetic energy into potential energies as seen below.

In Figure 10b, system energies for the 32nd MD/OPX cycle were plotted versus time corresponding to the system temperature shown in Figure 10a. Starting from comparatively low values computed for the energy-minimized configuration of previous cycle, bonded energies (i.e., bond, angle, dihedral and improper torsion energies) were found to increase significantly during stepwise heating of the system, whereas there are slight increases to the system nonbonded energies (i.e., electrostatic and van der Waals energies). As a result, heat supply from thermal bath (i.e., increase in system kinetic energy) is converted into system potential energies and system total energy is increased. After the gradual heating procedure, capsid energies level off as the system is equilibrated and stay nearly constant during short replica MD runs that are used for OPX. As for the OPX resulting configuration, it can lead to high potential energies, especially for nonbonded van der Waals and electrostatic energies, which are due to unphysical structures, such as overlapped atoms and stretched bonds and angles. They are seen as spikes in energy curves during early stage of system energy minimization. These spikes disappear and system potential energies decrease significantly as more energy minimization steps are applied, which prepare the system atomic configuration to be ready for MD thermalization of next cycle.

For the entire 200 ns MD/OPX simulation, kinetic and total energies of swollen CCMV capsid were collected approximately every 10 ns from the short replica MD runs of

MD/OPX cycles and plotted as shown in Figure 10c. The system kinetic energy was found to stay constant with small fluctuations, which suggests that the gradual heating and MD equilibration are sufficient to thermalize the energy-minimized OPX resulting configuration for running short replica MD runs and thus computing ensemble-average rate of change in system OPs for extrapolation. On the other hand, the system total energy was shown to decrease monotonically from 498,406 kcal/mol to 447,539 kcal/mol. This indicates that the system potential energy decreases accordingly along the trajectory. As the shrinkage of swollen CCMV capsid mostly involves large-scale rearrangements of its pentamers and hexamers through cooperative motions as described above, the system entropy is expected to stay roughly constant, and thus CCMV capsid shrinkage is an energy-driven process.

CONCLUSIONS

Optimized multiscale MD/OPX is applied to simulate viral STs, notably for CCMV capsid. Based on the AMA theory for dynamical nanosystems and all-atom description of simulated systems by using interatomic force fields, MD/OPX avoids the need for parameter recalibration with each new application and therefore is generally applicable to all nanostructures. It accelerates MD for long-time simulation of viruses and other large bionanosystems and captures nanoscale collective motions and atomistic fluctuations simultaneously.

As an extensively studied virus, CCMV was chosen as our model system for investigating the ST mechanisms of viral capsids. Insights into the stabilities of the native and swollen states of CCMV capsid in vacuum were first obtained through short-time MD simulation. With the results showing that native CCMV capsid becomes stable after short, small shrinkage, whereas its swollen state undergoes significant shrinkage over a timescale that is much longer than 10 ns, long-time MD/OPX simulation was run on the swollen state with 200 ns dynamics of its shrinkage captured. Shrinkage of swollen CCMV capsid was found to be an energy-driven, symmetry-breaking process that involves large-scale translation and rotation of pentamers and hexamers in the capsid. The capsomeres undergo cooperative motions through strongly coupled allosteric interactions during capsid shrinkage. As a result, viral STs start locally and then propagate across the capsid, i.e., they proceed via intermediate states that are not constrained to the capsid symmetry. This suggests that it is not appropriate to use symmetry-constrained models to study the pathways and mechanisms of viral STs.

In ongoing studies, modules in MD/OPX have been developed to redistribute water molecules and ions around nanostructures for simulating systems solvated in aqueous media. It will be demonstrated on the swelling of native CCMV capsid in a host medium with pH 7.0 and ionic strength equal to 0.2 M.⁴⁹ Such behaviors have been observed through our preliminary simulations and they agree well with experimental data. Given the power that MD/OPX can be applied to simulate viral STs, we suggest it will have the capability for computer-aided design of antiviral drugs and vaccines, and nanocapsules for delivery of therapeutic agents to diseased tissues.

MATERIALS AND METHODS

CCMV Capsid Structures and MD Simulations

Native CCMV capsid was generated by orienting 60 copies of the X-ray crystal structure of its protomer (PDB ID: 1CWP)² according to the icosahedral symmetry. Swollen state of the capsids was constructed by taking its pentamers and hexamers through rigid-body transformations from their native configurations as the following⁵⁰: translating pentamers by 24 Å radially outward and rotating them counter-clockwise by 9° around their fivefold axes, translating hexamers by 21 Å radially outward, and rotating them counter-clockwise by 8° around their threefold axes.

VMD⁶⁴ was used to create the capsid structural topology and NAMD⁶⁵ was implemented to simulate the native and swollen states of CCMV capsid in vacuum by using CHARMM22 force field^{66,67} for capsid proteins. Both simulations started with an initial energy minimization for 10,000 steps using the conjugate gradient algorithm, with which the system potential energies decrease to local minima and stay constants. Two energy-minimized structures were then gradually heated to 298.15 K and equilibrated under this temperature for 20 ps. Product MD runs capturing 10 ns dynamics of the two capsid states were obtained to investigate their stability. A multiple-time-stepping algorithm⁶⁵ was used for the MD simulations: bonded interactions were computed for every timestep, short-range nonbonded interactions every two timesteps, and long-range electrostatic interactions every four timesteps.

Construction of Order Parameters from Atomic Configurations

Consider a nanostructure embedded in a box (a cube for simplicity of presentation) of volume L^3 . Basis functions $u_k(x)$ (e.g., orthogonal polynomials or harmonic functions) labeled with integer index k are introduced such that

$$\int_{-L/2}^{L/2} dx u_k(x) u_{k'}(x) = \delta_{kk'} \quad (1)$$

for Kronecker delta $\delta_{kk'}$. Composite functions $U_{\underline{k}}(\vec{s})$ are defined such that

$$U_{\underline{k}}(\vec{s}) = u_{k_1}(x) u_{k_2}(y) u_{k_3}(z), \quad (2)$$

where $\vec{s} = (x, y, z)$ for box centered at $\vec{s} = \vec{0}$. By using $U_{\underline{k}}(\vec{s})$, system collective modes can be constructed as $\vec{U}_{\underline{k}}(\vec{s}^0) = \{\vec{U}_{\underline{k}}(\vec{s}_1^0), \dots, \vec{U}_{\underline{k}}(\vec{s}_N^0)\}$ with $\vec{s}^0 = \{\vec{s}_1^0, \dots, \vec{s}_N^0\}$ and the nanostructure \vec{s} is considered to be deformation of a reference configuration \vec{s}^0 :

$$\vec{s}_i = \sum_{\underline{k}} U_{\underline{k}}(\vec{s}_i^0) \vec{\Psi}_{\underline{k}} + \vec{\sigma}_i, \quad (3)$$

where $\vec{\sigma}_i$ is the residual due to finite truncation of k sum and $\vec{\Psi}_{\underline{k}}$ are system order parameters (OPs). Assume m_i is the mass of atom i and $m = \frac{1}{N} \sum_{i=1}^N m_i$. We determine $\vec{\Psi}_{\underline{k}}$ to minimize the mass-weighted root mean square residuals (RMSR), i.e., $\sqrt{\frac{1}{N} \sum_{i=1}^N \frac{m_i}{m} \vec{\sigma}_i^2}$, which yields

$$\sum_{\underline{k}} B_{\underline{q}\underline{k}} \vec{\Psi}_{\underline{k}} = \frac{L^3}{N} \sum_{i=1}^N \frac{m_i}{m} U_{\underline{q}}(\vec{s}_i^0) \vec{s}_i, \quad (4)$$

$$B_{\underline{q}\underline{k}} = \frac{L^3}{N} \sum_{i=1}^N \frac{m_i}{m} U_{\underline{q}}(\vec{s}_i^0) U_{\underline{k}}(\vec{s}_i^0).$$

The $\vec{\sigma}_i$ contribution is neglected in arriving at this definition of $\vec{\Psi}_{\underline{k}}$ as $\vec{\sigma}_i$ fluctuates with i and hence with space, whereas the basis functions that capture overall nanostructural features vary smoothly by design. When most of the space in the system is occupied with atoms, the i sum is essentially a Monte Carlo integration. The orthogonality of the normalized basis functions implies that $B_{\underline{q}\underline{k}} \approx \delta_{\underline{q}\underline{k}}$ and Eq. (4) can be approximated as

$$\vec{\Psi}_{\underline{q}} \approx \frac{L^3}{N} \sum_{i=1}^N \frac{m_i}{m} U_{\underline{q}}(\vec{s}_i^0) \vec{s}_i. \quad (5)$$

Therefore, dimensionality reduction for nanostructures from the N -atom configuration to M OPs is achieved through

$$\vec{s}_i, \{i = 1, \dots, N\} \rightleftharpoons \vec{\Psi}_{\underline{k}}, \{\underline{k} = \underline{k}_1, \dots, \underline{k}_M\}. \quad (6)$$

In the above formulation, atomic coordinates of a reference configuration are used to construct the nanostructure collective modes and their summation given by Eq. (3) results in a new configuration that the system can evolve to. Instead atomic displacements calculated from two known configurations of the nanostructure can be used to construct its collective modes and their summations weighted by OPs would describe system coherent motions directly.⁴⁰

For MD/OPX simulation of swollen CCMV capsid, 3³ OPs were constructed by using Legendre polynomials of atomic coordinates over order (0, 1, 2) in X, Y, and Z-directions with Eq. (4) solved rigorously. Low-order Legendre polynomials were selected because they vary smoothly in space and thus can capture nanoscale features of viruses, such as viral position, orientation, size, shape, and overall conformation. The automatically constructed OPs were demonstrated to be slowly varying and collisions and capable of capturing the nanoscale dynamics of capsomers during CCMV capsid STs.²³

MD/OPX Optimization and Application to Swollen CCMV Capsid

In our earlier study,²³ MD/OPX was demonstrated on swollen CCMV capsid. Analysis results of the simulation for 1 ns are shown to agree well with those obtained from direct MD run. Since then, MD/OPX has been further optimized by (1) averaging a set of short replica MD runs with random atomic velocity initializations to compute ensemble-average rates of change in OPs, instead of using one single MD trajectory, (2) updating the reference configuration for constructing system order parameters at a certain frequency such that the latest collective motions of the structure can be effectively captured, (3) improving the maturing of OPX resulting structure by applying energy minimization, graduate heating, and short-time MD equilibration before running short replica MD bursts for OPX, and (4) choosing optimal OP timestep for extrapolation and atomic acceleration indicators to evaluate the OPX resulting structure to achieve adaptive variation of MD/OPX parameters.

MD/OPX simulation of swollen CCMV capsid started with the resultant structure of its MD simulation at 1 ns as described above and proceeded with cycles of short replica MD runs and projection of the atomic structure by extrapolating its ensemble-averaged OPs over long time. In each cycle, ten 500 fs replica MD runs with random atomic velocity initializations under 298.15 K were obtained for computing the ensemble-average rates of change in capsid OPs, which are then used to extrapolate the OPs over long time. The newly obtained OPs were taken to reconstruct atomic configuration of the capsid that will go through 1000-step energy minimization, six-stepwise graduate heating to 298.15 K and 5 ps MD equilibration. atomic accelerations of the resulting structure were computed as indicators to determine whether the structure is mature for the next MD/OPX cycle, and the timestep for extrapolation of OPs is adjusted adaptively to ensure the simulation is stable. By repeating such cycles, swollen CCMV capsid was simulated for 200 ns in vacuum with its shrinkage captured.

The OP timestep obtained from adaptive MD/OPX cycles was found to undergo periodic oscillations and its average for the entire simulation was determined to be 60 ps. With this, the ratio of average OP timestep to the time interval of short MD bursts is largely increased to 120, compared with 10 obtained from the simulation of previous study²³ by using only a single short MD run for OPX. When comparing the simulation time of MD/OPX to that of one single MD run, the overall speedup of MD/OPX over MD is by a factor of 6. However, as 10 short replica MD runs were used in MD/OPX for extrapolating the OPs, ensemble-average effects have been accounted for and our MD/OPX becomes 60 times faster than an ensemble of 10 replica MD runs. The MD/OPX simulation was run on Indiana University Big Red cluster with performance of 0.06 days/ns when using 256 processors and 0.11 days/ns for 128 processors.

The authors are grateful for the computing time provided by Indiana University Big Red supercomputer.

REFERENCES

- Adolph, K. W. *J Gen Virol* 1975, 28, 147–154.
- Speir, J. A.; Munshi, S.; Wang, G. J.; Baker, T. S.; Johnson, J. E. *Structure* 1995, 3, 63–78.
- Liepold, L. O.; Revis, J.; Allen, M.; Oltrogge, L.; Young, M.; Douglas, T. *Phys Biol* 2005, S166–S172.
- Speir, J. A.; Bothner, B.; Qu, C.; Willits, D. A.; Young, M. J.; Johnson, J. E. *J Virol* 2006, 80, 3582–3981.
- Canady, M. A.; Tihova, M.; Hanzlik, T. N.; Johnson, J. E.; Yeager, M. *J Mol Biol* 2000, 299, 573–584.
- Canady, M. A.; Tsuruta, H.; Johnson, J. E. *J Mol Biol* 2001, 311, 803–814.
- Wikoff, W. R.; Conway, J. F.; Tang, J.; Lee, K. K.; Gan, L.; Cheng, N.; Duda, R. L.; Hendrix, R. W.; Steven, A. C.; Johnson, J. E. *J Struct Biol* 2006, 153, 300–306.
- Belnap, D. M.; Filman, D. J.; Trus, B. L.; Cheng, N. Q.; Booy, F. P.; Conway, J. F.; Curry, S.; Hiremath, C. N.; Tsang, S. K.; Steven, A. C.; Hogle, J. M. *J Virol* 2000, 74, 1342–1354.
- Hogle, J. M. *Annu Rev Microbiol* 2002, 56, 677–702.
- Freddolino, P. L.; Arkhipov, A. S.; Larson, S. B.; McPherson, A.; Schulten, K. *Structure* 2006, 14, 437–449.
- Speelman, B.; Brooks, B. R.; Post, C. B. *Biophys J* 2001, 80, 121–129.
- Phelps, D. K.; Rossky, P. J.; Post, C. B. *J Mol Biol* 1998, 276, 331–337.
- Harries, D.; May, S.; Gelbart, W. M.; Ben-Shaul, A. *Biophys J* 1998, 75, 159–173.
- Arkhipov, A.; Freddolino, P. L.; Schulten, K. *Structure* 2006, 1767–1777.
- Tama, F.; Brooks, C. L. *J Mol Biol* 2002, 318, 733–747.
- Tama, F.; Brooks, C. L. *J Mol Biol* 2005, 345, 299–314.
- Van Vlijmen, H. W. T.; Karplus, M. *J Mol Biol* 2005, 350, 528–542.
- Roy, A. S.; Miao, Y.; Ortoleva, P. *J Comput Chem* 2008. In Review.
- Zhang, D. Q.; Konecny, R.; Baker, N. A.; Mccammon, J. A. *Biopolymers* 2004, 75, 325–337.
- Konecny, R.; Trylska, J.; Tama, F.; Zhang, D. Q.; Baker, N. A.; Brooks, C. L.; Mccammon, J. A. *Biopolymers* 2006, 82, 106–120.
- Sayed-Ahmad, A.; Miao, Y.; Ortoleva, P. *Commun Comput Phys* 2008, 3, 1100–1116.
- Miao, Y.; Ortoleva, P. *J Chem Phys* 2006, 125, 44901.
- Miao, Y.; Ortoleva, P. *J Comput Chem* 2008, 30, 423–437.
- Pankavich, S.; Miao, Y.; Ortoleva, J.; Shreif, Z.; Ortoleva, P. *J Chem Phys* 2008, 029822.
- Chandrasekhar, S. *Astrophys J* 1943, 97, 255–262.
- Deutch, J. M.; Oppenheim, I. *Faraday discuss. Chemical Society: London*, 1987, pp 1–20.
- Deutch, J. M.; Ross, J.; Ortoleva, P. J.; Hudson, S. *J Chem Phys* 1972, 57, 4327.
- Shea, J. E.; Oppenheim, I. *J Phys Chem* 1996, 100, 19035–19042.
- Shea, J. E.; Oppenheim, I. *Phys A* 1997, 247, 417–443.
- Ortoleva, P. J. *J Phys Chem B* 2005, 109, 21258–21266.
- Peters, M. H. *J Stat Phys* 1999, 94, 557–586.
- Peters, M. H. *J Chem Phys* 1999, 110, 528–538.
- Zwanzig, R. *Nonequilibrium Statistical Mechanics*. Oxford University Press: New York, 2001.
- Shreif, Z.; Ortoleva, P. *J Stat Phys* 2008, 669–685.
- Miao, Y.; Ortoleva, P. *J Chem Phys* 2006, 125, 214901.
- Chang, R.; Ayton, G. S.; Voth, G. A. *J Chem Phys* 2005, 122, 244716.

37. Ayton, G. S.; Voth, G. A. *J Struct Biol* 2007, 157, 570–578.
38. Kevrekidis, I. G.; Gear, C. W.; Hummer, G. *AIChE J* 2004, 50, 1346–1355.
39. Hummer, G.; Kevrekidis, I. G. *J Chem Phys* 2003, 118, 10762–10773.
40. Miao, Y.; Ortoleva, P. J. *Phys Rev Lett* 2009, In press
41. Lange, O. F.; Grubmuller, H. *J Phys Chem B* 2006, 110, 22842–22852.
42. Balsera, M. A.; Wriggers, W.; Oono, Y.; Schulten, K. *J Phys Chem* 1996, 100, 2567–2572.
43. Kitao, A.; Go, N. *Curr Opin Struct Biol* 1999, 9, 164–169.
44. Clarage, J. B.; Romo, T.; Andrews, B. K.; Pettitt, B. M.; Phillips, G. N. *Proc Natl Acad Sci USA* 1995, 92, 3288–3292.
45. Zhang, Z. Y.; Wriggers, W. *J Phys Chem B* 2008, 112, 14026–14035.
46. Dey, B. K.; Rabitz, H.; Askar, A. *J Chem Phys* 2003, 119, 5379–5387.
47. Bancroft, J. B.; Hiebert, E. *Virology* 1967, 32, 354–356.
48. Brumfield, S.; Willits, D.; Tang, L.; Johnson, J. E.; Douglas, T.; Young, M. *J Gen Virol* 2004, 85, 1049–1053.
49. Miao, Y.; Johnson, J.; Ortoleva, P. 2009, *J Phys Chem B*. In review.
50. Liu, H. J.; Qu, C. X.; Johnson, J. E.; Case, D. A. *J Struct Biol* 2003, 142, 356–363.
51. Ortoleva, P. *Nonlinear Chemical Waves*, Wiley: NY, 1992.
52. Ortoleva, P.; Chen, Y.; Chen, W. *Fractals and dynamic systems in geoscience*; Jörn, H., Ed. Springer-Verlag: NY, 1994; pp 283–305.
53. Kadau, K.; Germann, T. C.; Lomdahl, P. S.; Holian, B. L. *Science* 2002, 296, 1681–1684.
54. Catti, M.; Ibberson, R. M. *J Phys Chem B* 2002, 106, 11916–11921.
55. Guerin, T.; Bruinsma, R. *Phys Rev E* 2007, 76, 061911.
56. Caspar, D. L. D. *Biophys J* 1980, 32, 103–138.
57. Conway, J. F.; Wikoff, W. R.; Cheng, N.; Duda, R. L.; Hendrix, R. W.; Johnson, J. E.; Steven, A. C. *Science* 2001, 292, 744–748.
58. Rader, A. J.; Vlad, D. H.; Bahar, I. *Structure* 2005, 13, 413–421.
59. Lee, K. K.; Gan, L.; Tsuruta, H.; Hendrix, R. W.; Duda, R. L.; Johnson, J. E. *J Mol Biol* 2004, 340, 419–433.
60. Jacrot, B. *J Mol Biol* 1975, 95, 433–446.
61. Klug, W. S.; Bruinsma, R. F.; Michel, J. P.; Knobler, C. M.; Ivanovska, I. L.; Schmidt, C. F.; Wuite, G. J. L. *Phys Rev Lett* 2006, 97, 228101.
62. Fricks, C. E.; Hogle, J. M. *J Virol* 1990, 64, 1934–1945.
63. Tsang, S. K.; Danthi, P.; Chow, M.; Hogle, J. M. *J Mol Biol* 2000, 296, 335–340.
64. Humphrey, W.; Dalke, A.; Schulten, K. *J Mol Graph* 1996, 14, 33.
65. Phillips, J. C.; Braun, R.; Wang, W.; Gumbart, J.; Tajkhorshid, E.; Villa, E.; Chipot, C.; Skeel, R. D.; Kale, L.; Schulten, K. *J Comput Chem* 2005, 26, 1781–1802.
66. Mackerell, A. D.; Bashford, D.; Bellott, M.; Dunbrack, R. L.; Field, M. J.; Fischer, S.; Gao, J.; Guo, H.; Ha, S.; Joseph, D.; Kuchnir, L.; Kuczera, K.; Lau, F. T. K.; Mattos, C.; Michnick, S.; Nguyen, D. T.; Ngo, T.; Prodhom, B.; Roux, B.; Schlenkrich, M.; Smith, J.; Stote, R.; Straub, J.; Wiorkiewicz-Kuczera, J.; Karplus, M. *FASEB J* 1992, 6, A143–A143.
67. Mackerell, A. D.; Bashford, D.; Bellott, M.; Dunbrack, R. L.; Evanseck, J. D.; Field, M. J.; Fischer, S.; Gao, J.; Guo, H.; Ha, S.; Joseph-Mccarthy, D.; Kuchnir, L.; Kuczera, K.; Lau, F. T. K.; Mattos, C.; Michnick, S.; Ngo, T.; Nguyen, D. T.; Prodhom, B.; Reiher, W. E.; Roux, B.; Schlenkrich, M.; Smith, J. C.; Stote, R.; Straub, J.; Watanabe, M.; Wiorkiewicz-Kuczera, J.; Yin, D.; Karplus, M. *J Phys Chem B* 1998, 102, 3586–3616.

Reviewing Editor: J. A. McCammon